Journal of Applied Fluid Mechanics, Vol. 16, No. 4, pp. 655-670, 2023.
Available online at www.jafmonline.net, ISSN 1735-3572, EISSN 1735-3645.
https://doi.org/10.47176/jafm.16.04.1466

Various Wavy Leading-Edge Protuberance on Oscillating Hydrofoil Power Performance

A. Abbasi[1], H. Ghassemi[1,2†], H. Ghafari[1] and G. He[2]

[1] *Marine and Hydrokinetic Energy Group, Department of Maritime Engineering, Amirkabir University of Technology, Tehran, Iran*
[2] *International School of Ocean Science and Engineering, Harbin Institute of Technology, Weihai, China*

†*Corresponding Author Email: gasemi@aut.ac.ir*

(Received July 24, 2022; accepted December 12, 2022)

ABSTRACT

This paper is presented to compare various wavy leading-edge protuberances on oscillating hydrofoil performance and power efficiency. The unsteady turbulent 3D flow simulations were carried out by using the StarCCM+ software. The 3D hydrofoil with a straight at the leading-edge is a NACA0015 section with a chord of 0.24 m and an aspect ratio of 7. Four new types of hydrofoils are proposed with wavy leading-edge protuberance. The RANS equations with the realizable k–ε turbulence model are used to predict the turbulent flow around the hydrofoil under different conditions. In order to validate, a comparison of the numerical results of the forces coefficients and power efficiency of non-protuberance oscillating hydrofoil are shown in good agreement with experimental data. Then, four new profiles on the leading-edge of the hydrofoils are simulated and many results of the pressure distribution, vorticity contour, streamline velocity, and power coefficient for five hydrofoil types are presented and discussed. It is concluded that the hydrofoil of Type-M can achieve constantly higher efficiency of over 46% by employing appropriate heave and pitch amplitudes.

Keywords: Leading-edge protuberance; Oscillating hydrofoils; Pressure distribution; Hydrodynamic performance; Power efficiency.

NOMENCLATURE

b	Span	P_Y	heaving power
C_X	horizontal forces coefficient	P_θ	pitching power
C_Y	vertical forces coefficient	P	total power
C_M	moment coefficient	$\bar{P}$	total average extraction power
C_{P_Y}	heave power coefficient	p	pressure
C_{P_θ}	pitch power coefficient	U_∞	inflow velocity
C_P	power coefficient	u	flow velocity
$C_{pressure}$	pressure coefficient	V_Y	heaving velocity
C	chord	α	angle of attack
d	total extend of the hydrofoil vertical motion	δ	Kronecker delta
		η	power efficiency
f	oscillating frequency	θ	pitch amplitude
f^*	reduced frequency	μ	dynamic viscosity
F_X	horizontal force along the X-axis	ρ	fluid density
F_Y	vertical force along the Y-axis	ϕ	phase angle between the heaving and pitching motion
h	heave amplitude		
M	pitching moment	ω	angular velocity

1. INTRODUCTION

Many countries have planned and mapped out renewable energy for optimal use of natural resources. The UK Energy Research Centre (UKERC), in particular the marine energy research network, developed a route map for marine renewable energy research at the national and EU level. The world energy council provided an excellent survey of a road map on energy resources, wave energy converters technologies, and recommendations for the way forward in terms of R&D and commercial exploitation (Mueller and Wallace 2006).

More than thousands of inventions are involved in several forms of marine energy processing products. In recent years, renewable energy from the ocean has been widely explored; including ocean waves, sunlight and tidal energy, and increasingly scientists have focused on the utilization of ocean energy (Qi *et al.* 2019). Energy harvesting machinery plays a significant part in the usage of tidal power. Such systems may be categorized into three groups based on the operating principle: oscillating hydrofoils, horizontal-axis tidal turbines (HATT) and vertical-axis tidal turbines (VATT) (Xiao and Zhu 2014; Rostami and Armandei 2017; Abbasi *et al.* 2018; Segura *et al.* 2018). The oscillating hydrofoils have a lower tip speed ratio (TSR) than the turbine harvesters, have a low marine environment effect, are appropriate for shallow water are perfect for rating power expansion (Liu *et al.* 2019; Wu *et al.* 2020). The oscillating hydrofoil absorbs energy from the fluid by heaving and pitching motions (Dahmani and Sohn 2020). Figure 1 shows the conventional oscillating hydrofoil that is used to harvest the hydrokinetic energy of oceans.

Comprehensive works carried out on the coupled oscillating motions (heaving and pitching motions) of a single hydrofoil and two tandem hydrofoils by Kinsey *et al.* (2008-2014) (Kinsey and Dumas 2008, 2012, 2014; Kinsey *et al.* 2011). They presented many results on the hydrodynamic characteristics and power extractions of the 2D and 3D oscillating hydrofoils. Their results indicated that the heaving amplitude and frequency, unlike the geometrical parameters, have a major effect on the efficiency of the hydrofoil. Karakas and Fenercioglu (2016) investigated the influence of limited flow on the performance of an oscillating hydrofoil power generator. In this study, the flow patterns around and in the near wake of a flat plate positioned between two side walls are recorded using the PIV technique in uniform flow at Re=10000. To prediction of flapping foil hydrodynamic performance, a transitional model for RANS equations was used by Erfort *et al.* (2019). They concentrated on the intermittency and momentum thickness Reynolds number model based on correlation.

Nowadays, many researchers have been investigating energy power extraction with the oscillating hydrofoil. Javed *et al.* (2018) explored the operation of a semi-passive flapping hydrofoil flow

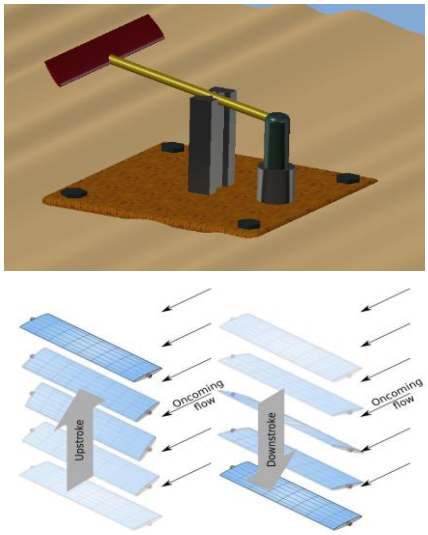

Fig. 1. Heave and pitch oscillating hydrofoil.

energy harvester at Reynolds numbers ranging from 5000 to 50,000 using a 2-D numerical solution technique. In order to augment the energy power efficiency, one object can be focused on the effect of the leading-edge shape to reach better the flow streamlines and vortex (Xu *et al.* 2019). Mumtaz Qadri *et al.* (2019) investigated an experimental study of a passively flapping foil in energy harvesting mode. A water tunnel test-rig was designed and constructed to study this notion, in which a flat plate foil made of plexiglass executes pitch and heave motion. Ribeiro *et al.* (2020) evaluated the performances of vortex dynamics and Reynolds number effects on an oscillating hydrofoil in energy harvesting mode. They investigated oscillating heave and pitch motions on an elliptical shape of the hydrofoil by large-eddy simulation at different Reynolds numbers between 1000 and 50000. Jamil *et al.* (2020) investigated the performance of a semi-active oscillating airfoil linked with a piezoelectric transducer. In its translational phase, the airfoil is supported by a spring, damper, and piezoelectric transducer combination. Experimental and numerical investigations of the oscillating hydrofoil under the fully-activated strategy and different test conditions were carried out by Liu *et al.* (2020).

Derazgisoo *et al.* (2019) conducted a numerical study of unsteady flows with forced periodical oscillation around hydrofoils. Their results showed a good precision of the locally power-law preconditioning method. A newly improved oscillating-wing wind and hydropower generator was studied on a single 2D NACA0014 wing by Ashraf *et al.* (2011). Their results demonstrated an approximately 17% increase in power generation versus 15% for sinusoidal motion. Besides, it was shown in tandem configurations compared to one hydrofoil in both sinusoidal and non-sinusoidal motions the power extraction efficiency was decreased by 20% per hydrofoil. Comparing tandem configurations with one hydrofoil in both sinusoidal

and non-sinusoidal motions showed that the power extraction efficiency was reduced by 20% per hydrofoil. The propulsive properties of a NACA012 hydrofoil are quantitatively studied by Li *et al.* (2022), inspired by fish kinematics. A numerical study was employed on coupled heave and pitch motion of oscillating hydrofoil using StarCCM+ software (Abbasi *et al.* 2021). They investigate ted hydrodynamic characteristics of hydrofoils and analyzed flow patterns in various flow velocities and reduced frequency. Also, the numerical simulations on the 2D oscillating hydrofoil intended to obtain an effective angle of attack (He *et al.* 2021). Pourmahdavi *et al.* (2019) worked on the power extraction mechanism of the flapping foil hydrokinetic turbine at the reduced frequency range of 0.06-0.18. The results showed, at a reduced frequency of 0.11, the maximum energy extraction efficiency reaches about 35.2%. Gunnarson *et al.* (2019) examined the pitching hydrofoil for five different linear models to predict a minor lateral alteration made by a hydrofoil undergoing biased pitch oscillations. The interaction between the vortex pattern and the cavitation shedding dynamics was modeled by large eddy simulation (Kanfoudi *et al.* 2017). There are many genus in the ocean that can serve as engineering inspiration and the humpback whale is one such species (Utama *et al.* 2020). The morphology of humpback whales' pectoral flippers inspired the concept of looking into the effects of leading-edge protuberances on hydrofoil results (Fig. 2). In comparison to other genus, the humpback whale is highly maneuverable despite its large size and rigid body. The humpback whale's flexibility has been due to its use of pectoral flippers (Johari *et al.* 2007). In addition to the unsteady motions associated with marine creatures, bionic curiosity has prompted a range of studies into unusual hydrofoil geometries (Dropkin *et al.* 2012). Wei *et al.* (2015) experimentally studied flow separation behavior and hydrodynamic characteristics of leading-edge tubercle hydrofoil at low Reynolds numbers. Srinivas *et al.* (2018) studied on flow characteristics of marine rudders with various wavy leading-edge configurations. Joseph *et al.* (2019) worked on the leading-edge tubercle effect on different types of wings at a low Reynolds number. Ganesh *et al.* (2019) numerically investigated the effect of surface blowing on aerodynamic characteristics of tubercle leading-edge wing considering different angles of attack and blowing velocity ratio. Li *et al.* (2021) investigated the theoretical and practical effect of wavy leading-edge protuberances on a Clark-y three-dimensional hydrofoil. The simulation is supplemented by a hybrid RANS-LES model in combination with the Zwart-Gerber-Belamri model. Reddy and Sathyabhama (2023) studied the influence of leading-edge protuberances on the aerodynamic performance of two different airfoils with low Reynolds numbers. Three protuberance forms were considered and the computational and experimental assessments were carried out at an angle of attack (AoA) of 0° to +20° and a Re of 10. Our laboratory of the Marine and Hydrokinetic Energy (MHK) group at the Maritime Engineering Department of AUT (Amirkabir University of Technology) was established to study the different types of the energy converters, Oscillating Water Column (OWC), Wavestar point absorbers, Tidal turbine and oscillating hydrofoils. The main objective of the current study is to apply a bionic perspective on oscillating hydrofoils for understanding the influence of different shapes at the leading-edge on its oscillating hydrodynamic performance and power extraction enhancement. Moreover, in this research, five different shapes of leading-edge tubercles based on various sinusoidal formulations were presented to enhance power performance by studying the flow field of the oscillating hydrofoils that were modified with inspiring nature. Therefore, this research is to investigate the number of crests on the leading-edge of oscillating hydrofoils with the same span length. The present work reports on numerical simulation concerning the power extraction of oscillating hydrofoil with a couple of motions of heave and pitch under five various configurations. Additionally, the numerical results are computed in wide range of reduced frequencies of 0.08-0.16. The remainder of

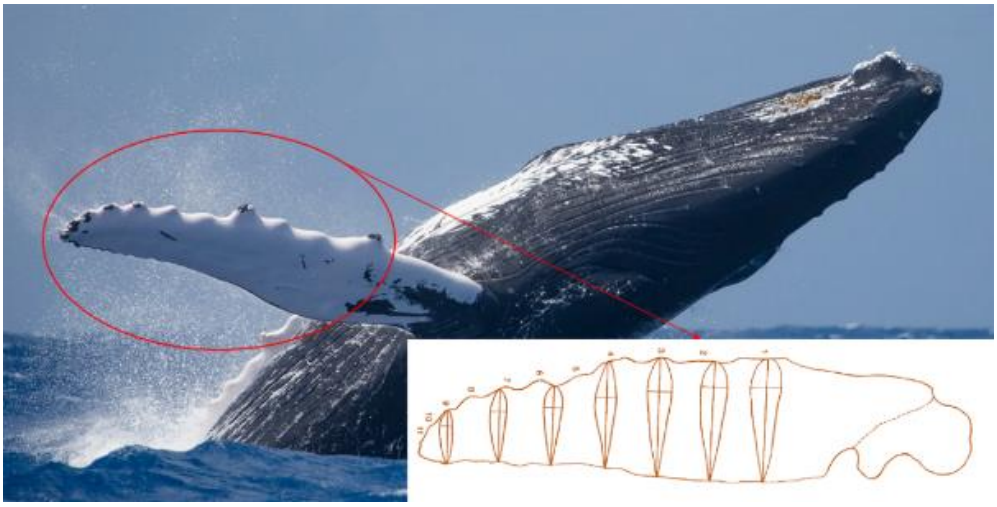

Fig. 2. Humpback whale with a form of cross-sections over the flipper (Fish and Battle 1995).

the paper is organized as follows. Section 2 describes the governing equations and motions description. Numerical implementation and validation are presented in Section 3. Section 4 presents the numerical results of the power coefficient under different reduced frequency for four new profiles at the leading-edge. Finally, the conclusions are drawn in Section 5.

2. COMPUTATIONAL METHODOLOGY

The commercial finite volume CFD code of the implementation used in this study is StarCCM+. Turbulent flows are influenced by irregular and fluctuating velocity fields. Transported quantities such as momentum and energy are mixed in these fluctuations. Fluctuations can occur on a variety of scales at various frequencies. Turbulent flows are more difficult to model directly in realistic engineering applications due to computer ability and solution time.

2.1 Governing Equations of Fluid

The governing equations for the turbulent incompressible flow encountered in this research are the Unsteady-state Reynolds-averaged Navier-Stokes (URANS) equations for the conservation of mass and momentum that presented in the following forms (Abbasi *et al.* 2019):

$$\frac{\partial \rho}{\partial t}+\frac{\partial}{\partial x_i}(\rho u_i)=0 \tag{1}$$

$$\begin{aligned}&\frac{\partial \rho u_j}{\partial t}+\frac{\partial}{\partial x_j}\left(\rho u_i u_j\right)\\&=-\frac{\partial P}{\partial x_i}\\&+\frac{\partial}{x_j}\left[\mu\left(\frac{\partial u_i}{\partial x_j}+\frac{\partial u_j}{\partial x_i}-\frac{2}{3}\delta_{ij}\frac{\partial u_l}{\partial x_l}\right)\right]\\&+\frac{\partial}{x_j}\left(-\rho\overline{x'_\iota x'_j}\right)\end{aligned} \tag{2}$$

where u_i is the flow velocity in the *i*-th direction, P is pressure, ρ is density of the fluid, μ is the turbulent viscosity, δ_{ij} indicates the Kronecker delta and $\rho\overline{x'_\iota x'_j}$ represent Reynolds stresses.

This method provides a solution for the mean flow variables and, as a result, reduces the computational effort. Eddy viscosity turbulence models like k-ε and k-ω and their derivatives are based on RANS, and the Reynolds-averaged approach is mostly usable for realistic engineering applications.

2.2 Motion Description

The functions of the heaving motion *h(t)* and pitching motion *θ(t)* acted on the hydrofoils are defined as:

$$h(t)=H_0\,sin(2\pi ft+\phi) \tag{3}$$

$$\theta(t)=\theta_0\,sin(2\pi ft) \tag{4}$$

where H_0 is the maximum heave amplitude, θ_0 is the maximum pitch amplitude and f is the oscillating frequency (Wu *et al.* 2020). In this study, the numerical simulation quantified the flow behavior and mechanism under the one cycle of hydrofoils motion. The reduced frequency is defined as:

$$f^*=\frac{fC}{U_\infty} \tag{5}$$

where U_∞ is inflow velocity.

The instantaneous horizontal and vertical forces coefficients acted on the oscillating foils are expressed as follows:

$$C_X(t)=\frac{F_X(t)}{0.5\rho U_\infty^2 bC} \tag{6}$$

$$C_Y(t)=\frac{F_Y(t)}{0.5\rho U_\infty^2 bC} \tag{7}$$

where ρ is the water density, F_X is the horizontal force along the X-axis and F_Y is the vertical force along the Y-axis (Wu *et al.* 2020).

The instantaneous power extraction $P(t)$ of the hydrofoil is calculated from the combined heaving power (P_Y) and pitching power (P_θ):

$$\begin{aligned}P(t)&=P_Y(t)+P_\theta(t)\\&=F_Y(t).V_Y(t)\\&+M(t).\omega(t)\end{aligned} \tag{8}$$

where V_Y is the heaving velocity, M is the pitching moment and ω is the angular velocity. Furthermore, the power coefficients of the hydrofoil are defined as follows:

$$C_{P_Y}(t)=\frac{P_Y(t)}{0.5\rho U_\infty^3 bC} \tag{9}$$

$$C_{P_\theta}(t)=\frac{P_\theta(t)}{0.5\rho U_\infty^3 bC} \tag{10}$$

$$C_P(t)=\frac{P(t)}{0.5\rho U_\infty^3 bC} \tag{11}$$

Consequently, to assess the performance of oscillating hydrofoil, power efficiency (η) is given as:

$$\eta=\frac{\bar{P}}{0.5\rho U_\infty^3 bd} \tag{12}$$

where $\bar{P}$ is the total average extraction power and *d* is the total extend of the hydrofoil vertical motion (Boudis *et al.* 2021).

Table 1 Main dimensions of the hydrofoil and operating conditions

Section type	Chord	Span	Heave amplitude	Pitch amplitude	Phase angle	Pitching axis
NACA0015	*C=0.24m*	*b=7C=1.68m*	H_0*=0.24m*	θ_0 *=75 deg*	ϕ *=90 deg*	*C/3 from LE*

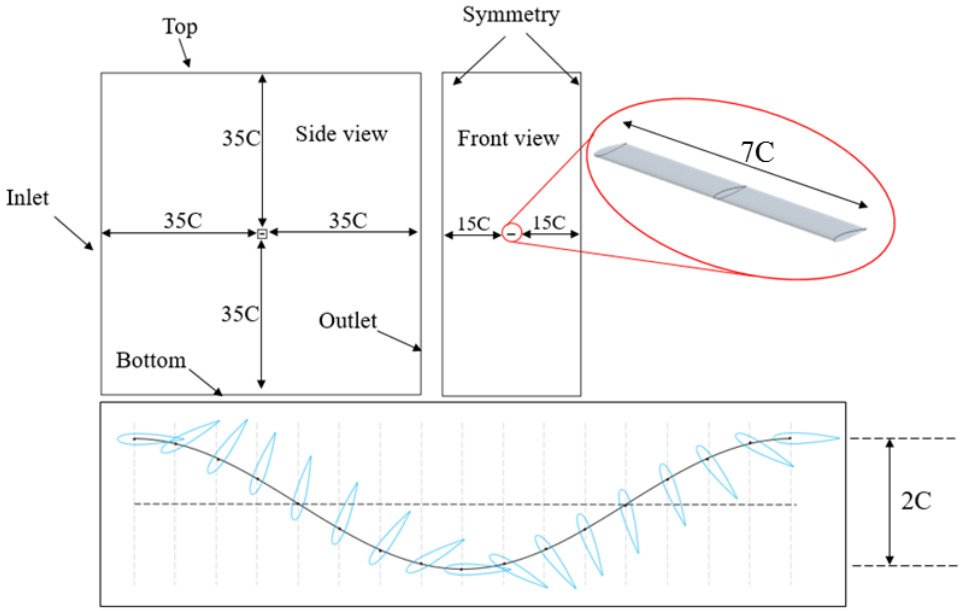

Fig. 3. Boundary conditions, computational domain and instant motion of the hydrofoil during one cycle.

3. NUMERICAL IMPLEMENTATION AND VALIDATION

3.1 Hydrofoil Geometry

The hydrofoil is selected as a 3D rectangular with symmetric section of the NACA0015, chord and span are *C* and *7C*, respectively, which the aspect ratio is equal 7. The hydrofoil is oscillating couple motions of heaving and pitching with amplitudes of H_0 *(=C)* and θ_0 *(=75^0)*, respectively. The pitching axis location is equal to *C/3* from leading-edge. Table 1 is given the main dimensions of the hydrofoil.

3.2 Boundary Conditions and Mesh Generation

The dimensions of the computational domain that use in this research are 70C for height, 70C for length and 30C for breadth. Furthermore, the upstream length is 35C and downstream length is 35C from hydrofoil. The hydrofoil is located at the central position of the x-z plane and x-y plane of the computational domain. The domain is discretized into 2.4×10^6 hexahedral grids that 1.2×10^6 grid generated for the region of hydrofoil motion includes 25 percent of all domain space, while 1.2×10^6 grid generated for another region of the domain. Figure 3 shows the computational domain, boundary conditions and instant motion of the hydrofoil during one cycle. According to Fig. 3 velocity inlet is selected for the inlet, top and bottom planes of the boundary conditions. Furthermore, the boundary conditions of side planes and the outlet plane are symmetry and pressure outlet, respectively.

Figure 4 is illustrated the mesh independency of the unsteady solution for power extraction efficiency of original oscillating hydrofoil at the reduced frequency of 0.14 and inflow velocity of 2 m/s. The result shows increasing mesh numbers leads to decreasing the power extraction efficiency. As shown in this figure, more than 2.5 million meshes, the power extraction efficiency is almost consent, so the number of 2.5 million meshes is adopted for calculations. Figure 5 shows the domain mesh, with close up view of mesh quality in the oscillation region of the hydrofoil, and the boundary layer around the hydrofoil surface. Figure 6 shows the contours of the Y^+ of the original hydrofoil. The majority of wall Y^+ values on hydrofoil surfaces are in the 30–90 range, which is acceptable for the present calculations.

3.3 Solver Set

In the present study, the realizable *k–ε* turbulence model in the StarCCM+ software is used. The time step is set at 0.0002s and 10 iterations per time step were calculated. At least the physical time that

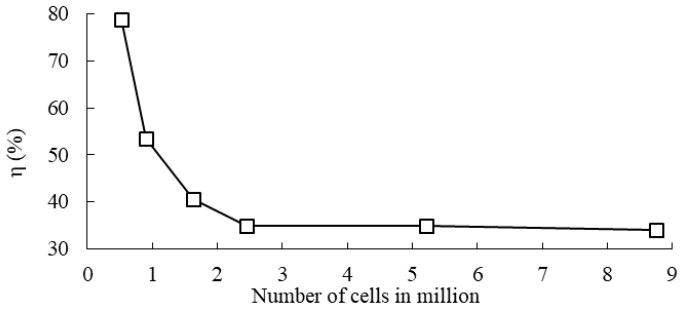

Fig. 4. Mesh independency for original hydrofoil at the reduced frequency of 0.14 and inflow velocity of 2m/s.

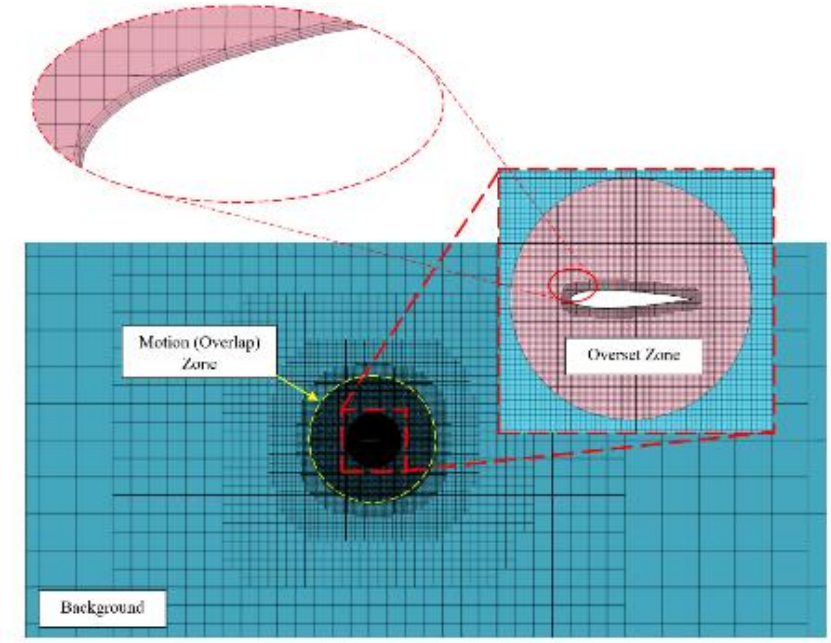

Fig. 5. Mesh generated over the original hydrofoil and domain.

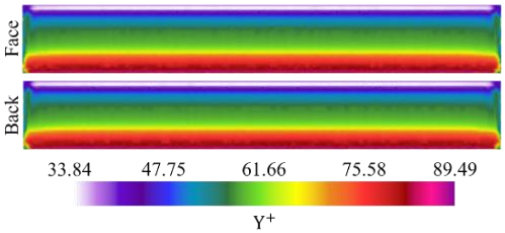

Fig. 6. Contours of Y^+ function.

computed for this simulation with seemed conditions is 10s. Based on Eq. (5) at the reduced frequency of 0.12 there are 10 motion cycles in 10 seconds that by considering this condition numerical model has an appropriate estimate from hydrofoil behavior.

3.4 Validation

To validate the force and power coefficients of the main hydrofoil, the present numerical results have been compared with the experimental data reported by Kinsey *et al*. (2008~2014) (Kinsey and Dumas 2008, 2012, 2014; Kinsey *et al.* 2011). The simulations have been performed at one cycle of hydrofoil oscillation considering the reduced frequency of 0.14, and a flow velocity of 2 m/s, as shown in Fig. 7. The present results the horizontal, vertical force and power coefficients are compared with experimental data. As shown in Fig. 7, there are good agreement between the present results and experimental data (Kinsey *et al*. 2011).

4. RESULTS AND DISCUSSIONS

4.1 Wavy Leading-Edge Protuberance

The main hydrofoil that called original designed from the NACA0015 section. Four different wavy leading-edge protuberance have been proposed base on the sinusoidal functions as follows:

- Type-O (Odd): the wavy leading-edge with 5 crests

- Type-E (Even): the wavy leading-edge with 4 crests

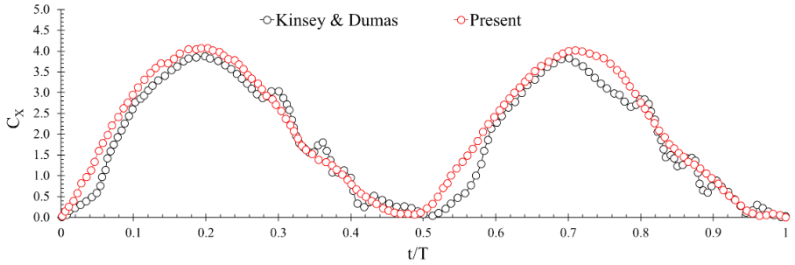

(a) The instantaneous horizontal force coefficient

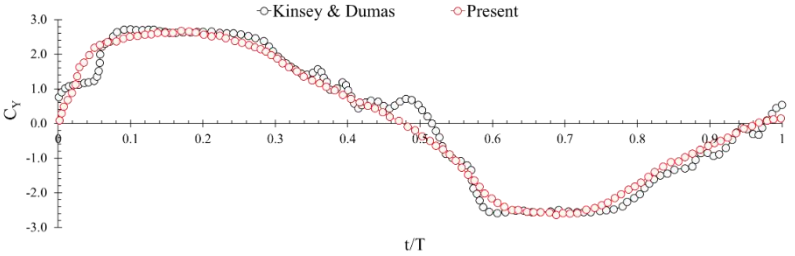

(b) The instantaneous vertical force coefficient

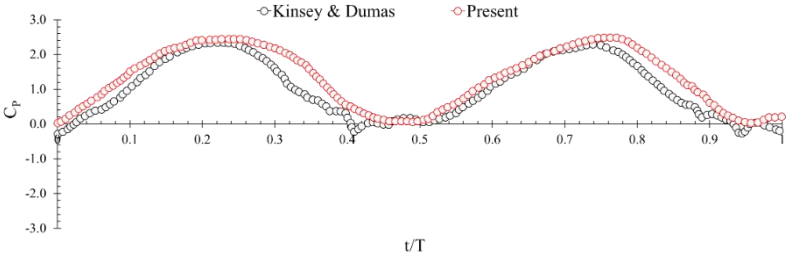

(c) The instantaneous power coefficients

Fig. 7. Comparison of horizontal, vertical force and power coefficients, ($f^* = 0.14, U_\infty$ =2m/s).

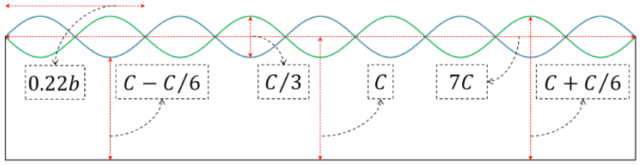

Fig. 8. Difference between original hydrofoil and modified hydrofoils.

- Type-M (Merge): the wavy leading-edge with 9 crests that produce from merging hydrofoils of Type-O and Type-E

- Type-S (Subtraction): the wavy leading-edge without crest that produces from subtracting hydrofoils of Type-O and Type-E

The amplitude of sinusoidal at leading-edge is chosen *C/6* and wave length is defined $\frac{2}{9}b$ ($\approx 0.22b$). Figure 8 indicates the original hydrofoil and formation procedure of modified hydrofoils and their crests based on the sinusoidal formulation. In addition, Fig. 9 illustrates four types of the hydrofoils with wavy leading-edge and the mathematical formulas are given for each of them.

4.2 Oscillation motion of the hydrofoils

The energy extraction from the sinusoidal coupled pitching and heaving motion of the five hydrofoils with different geometric at the leading-edge zone is investigated through RANS simulations at the reduced frequencies range of 0.08-0.16 and the constant inflow velocity of 2 m/s. So, to identify the effect of the non-dimensional frequency of sinusoidal motion and the related physics on the hydrodynamic performance of the oscillating hydrofoils, numerical simulations are completed for the main hydrofoil case without unusual leading-edge and hydrofoil cases with unusual leading-edge that oscillated in current as in the conventional pattern.

The oscillation motion of the hydrofoils is defined by different parameters. So, the effective Angle of Attack (AoA) of oscillating hydrofoil $\alpha(t)$ is defined at the pitching axis of the upstream hydrofoil as follow:

$$\alpha(t) = \theta(t) - arctan\left(\frac{V_Y(t)}{U_\infty}\right) \qquad (13)$$

Figure 10 shows the heaving motion (Eq. 3), pitching motion (Eq. 4) and effective AoA obtained from Eq. (13). Changes are shown at one cycle of oscillation,

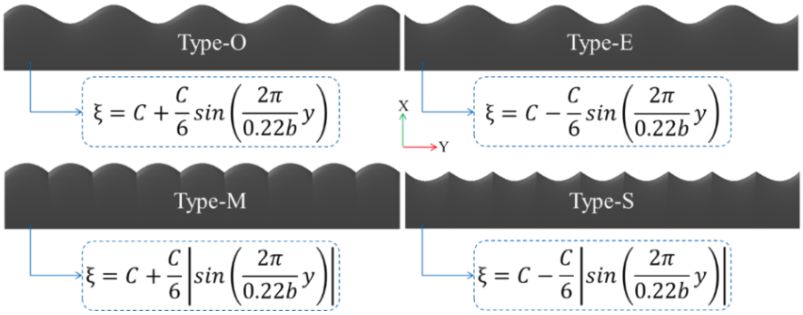

Fig. 9. Four types of wavy leading-edge protuberance of oscillating hydrofoils by sinusoidal functions.

the flow velocity of 2m/s and the oscillation frequency of $1s^{-1}$. Moreover, the heaving amplitude (H_0), pitching amplitude (θ_0) and phase angle between pitch and heave motions (ϕ) are 0.24 m, 75° and 90°, respectively. The maximum performance of oscillating hydrofoils is controlled by the optimum AoA which is dependent on the inflow velocity, pitching motion, and heaving velocity. The optimum AoA enhanced the power extraction energy.

4.3 Hydrodynamic Performance

The performance of oscillating hydrofoils based on the horizontal force coefficient (C_X), vertical force coefficient (C_Y) and moment coefficient (C_M) during one cycle are presented in Fig. 11. The results were obtained from conditions of f*=0.12 and inflow velocity of 2 m/s. Direct comparisons between the hydrodynamic parameter of considering case studies show the Type-M generated more thrust than other types (Type-O, Type-E, Type-S and original type) over predicting motion behavior. Moreover, the maximum and minimum peaks of C_M in the downward movement have occurred during the physical dimensionless times of 0.01-0.03 and 0.25-0.3, respectively. Also, in the upward movement, can be seen the minimum and maximum peaks of C_M have occurred during the physical dimensionless times of 0.55-0.57 and 0.77-0.82, respectively.

Figure 12 presents the comparison of the (total) power coefficient (C_P), heave power coefficient (C_{P_Y}) and pitch power coefficient (C_{P_θ}) between five hydrofoil types. Results were computed for a mean aspect ratio of 7, the phase angle of 90°, heaving amplitude of 0.24 m, pitching amplitude of 75°, reduced frequency of 0.12 and inflow velocity of 2 m/s. It can be found, that for one periodic cycle, the absorbed power by Type-M is greater than the other hydrofoils, besides the absorbed power by Type-S is less than that of original. The difference in peaks is more noticeable.

Furthermore, the hydrodynamic and power coefficients performance was examined for different reduced frequency (f^* =0.10, 0.12 and 0.14) and constant inflow velocity ($\bar{U}_\infty = 2\ m/s$). The result is reported in Table 2. It can be seen by increasing the reduced frequency from 0.10 to 0.12, the maximum torque, vertical force coefficient and mean of horizontal force coefficient increased. Also, by increasing the reduced frequency from 0.12 to 0.14, all coefficients decrease.

4.4. Pressure Distribution and Pressure Contour

Figure 13 indicates the pressure distribution contours at back and face sides for all five models at $f^* = 0.12$, $\bar{U}_\infty = 2$ m/s and at various angle of motions (0, 25, 50 and 75 degrees). The pressure distribution on the surfaces of modified hydrofoils in the spanwise direction is different from that of Original. On the face side of the modified leading-edge hydrofoils, the pressure distribution is lower in the downturn region and larger in the peak region, while no significant change can be found on the base line hydrofoil along the spanwise direction. Additionally, as the angle of motion increases, the magnitude of the pressure on the face side and back side of the modified hydrofoils increases. Furthermore, as can

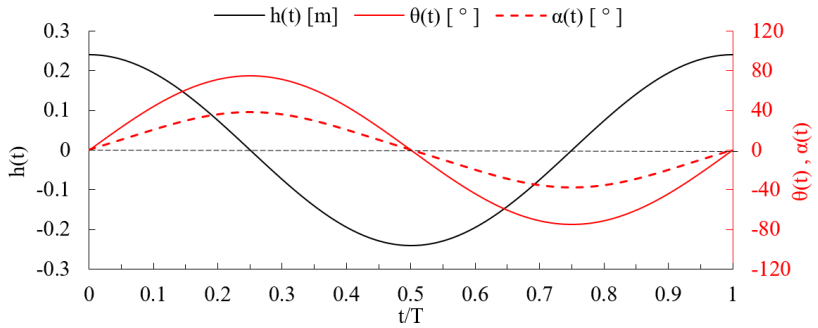

Fig. 10. Comparison of heaving motion, pitching motion and effective AoA during one cycle of oscillating motion.

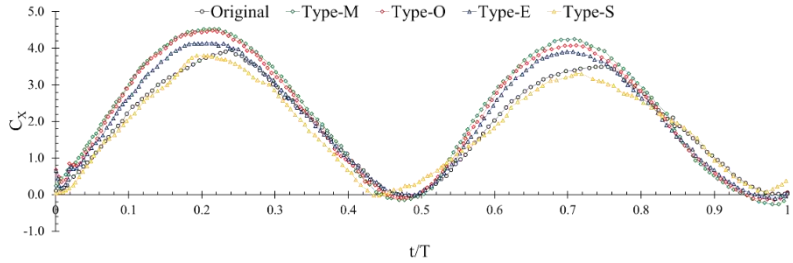

(a) Horizontal force coefficient

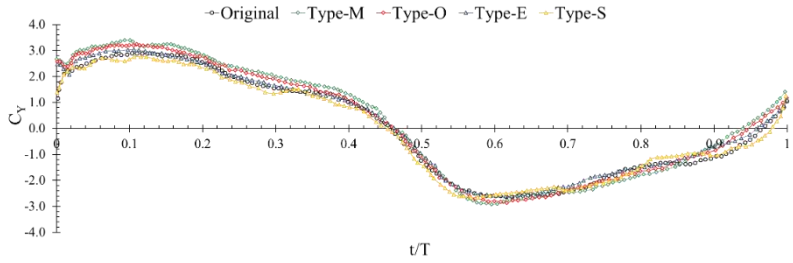

(b) Vertical force coefficient

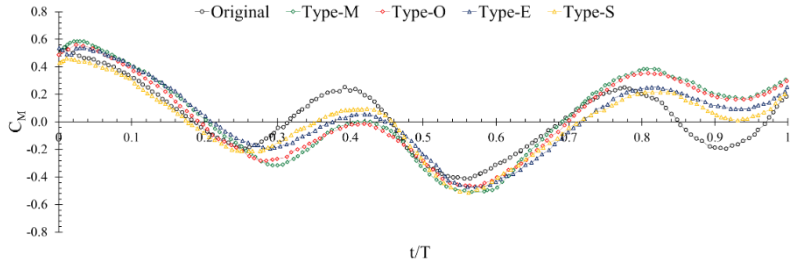

(c) Moment coefficient

Fig. 11. Comparison of horizontal and vertical force coefficient and moment coefficient between all five types of hydrofoils.

Table 2 Comparison of hydrodynamic and power coefficients between all five types of oscillating hydrofoils at different reduced frequencies

Model	$\overline{U}_\infty = 2\ m/s$						
	f^*	$\bar{C}_X$	$\hat{C}_Y$	$\hat{C}_M$	$\bar{C}_{P_\theta}$	$\bar{C}_{P_Y}$	$\bar{C}_P$
Original	0.10	1.624	2.769	0.488	0.159	0.766	0.925
	0.12	1.981	2.923	0.550	0.093	0.968	1.061
	0.14	1.783	2.852	0.513	0.188	0.812	1.001
Type-M	0.10	1.858	3.012	0.522	0.116	0.887	1.003
	0.12	2.209	3.395	0.585	0.184	1.048	1.232
	0.14	2.017	3.152	0.536	0.172	0.977	1.149
Type-O	0.10	1.794	2.868	0.510	0.152	0.846	0.998
	0.12	2.176	3.111	0.574	0.173	1.018	1.191
	0.14	1.910	2.995	0.526	0.186	0.941	1.128
Type-E	0.10	1.778	2.856	0.482	0.151	0.802	0.954
	0.12	2.104	3.015	0.551	0.173	0.990	1.163
	0.14	1.849	2.934	0.502	0.148	0.945	1.095
Type-S	0.10	1.581	2.644	0.448	0.150	0.762	0.912
	0.12	1.813	2.755	0.461	0.164	0.883	1.047
	0.14	1.702	2.711	0.456	0.143	0.841	0.986

be seen in the original hydrofoil, pressure distribution at the leading-edge section has a uniform structure because of the regular flow streamline. On the other hand, modified leading-edge of tubercle hydrofoils have non-uniform pressure distribution, especially in a wavy position. The main reason for this phenomenon is the flow behavior. It can be said, in modified hydrofoils flow separation occurs at the mid-section of the X-direction (negative pressure distribution at the back side) but at the same time flow is attached to peak regions. So, in the trough region i.e., between and lower than two peaks, the vortices have been developed to the trailing edge. At

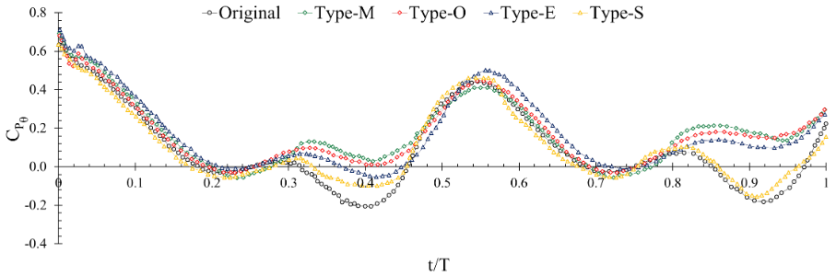

(a) Pitch power coefficient

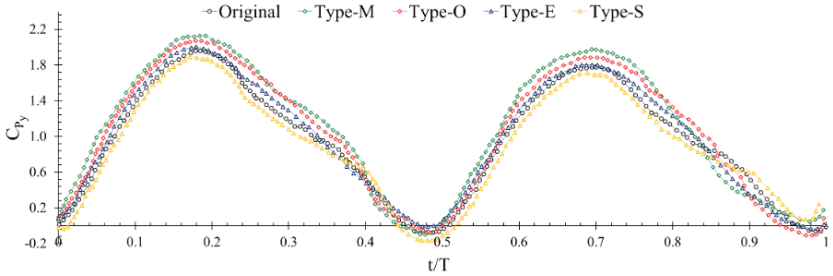

(b) Heave power coefficient

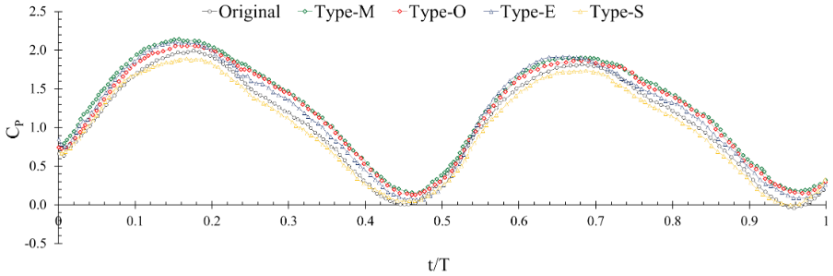

(c) Total power coefficient

Fig. 12. Comparison of generated power between all five types of oscillating hydrofoils, (f^*=0.12, $\overline{U}_\infty$ = 2 m/s).

least, the attached flow be seen near the trailing-edge that shows uniform pressure distribution in this position (positive pressure distribution at the back side).

To show the pressure coefficient of the back and face sides of the hydrofoil is an essential approach in the hydrodynamic performance. The pressure coefficient is expressed as follows:

$$C_{pressure} = (p - P_0)/0.5\rho U_0^2) \quad (14)$$

where p is local pressure on the hydrofoil, U_0 and P_0 are the velocity and pressure at the upstream of the hydrofoil, respectively.

Figure 14 shows the comparison of the pressure coefficient ($C_{pressure}$) at back and face sides of five types of the hydrofoil at various θ (10°, 20°, 40° and 60°), constant reduced frequency (0.12) and constant flow velocity (2 m/s) is presented. A hydrofoil shape produces hydrodynamic forces by a pressure difference over the upper and lower surfaces. As a result, at θ=60° the high positive pressure area is produced at the upper surface, and the thrust is improved at this moment. However, a low-pressure area near the lower surface of oscillating hydrofoils is generated. So, according to Fig. 14 the $C_{pressure}$ in the case of Type-M is found higher than others at the θ=60° and θ=40°, while at the θ=10° and θ=20° the $C_{pressure}$ of original hydrofoil is located on a high level than that of modified hydrofoils.

4.5. Streamline and Velocity Contour

The contour of streamline velocity of all five types of oscillating hydrofoils is shown in Fig. 15 under various dimensionless time and AoA under reduced frequency of $f^* = 0.12$ and inflow velocity of $\overline{U}_\infty = 2\ \mathrm{m/s}$. As the hydrofoils move, the speed of streamline, show a certain behavior during a cycle. The hydrodynamic operation of flow around the oscillating hydrofoils is periodical. The obtained the result clearly demonstrates that changing the leading-edge of the hydrofoil with sinusoidal changes the whole flow-field over the hydrofoils.

The progression of the separation line from the trailing edge to the leading-edge affects the flow characteristics of all five types of the hydrofoils studied here. At the leading-edge, the flow is totally separated above the maximum angle. Flow patterns with different motion angles can be generated by re-shaping with various modes. The flow field vortex phase properties at various AoA can be studied in this form. Contours of the velocity around the oscillating hydrofoils at $\overline{U}_\infty = 2\ \mathrm{m/s}$, f^*=0.12 and different AoA from 10° to 35° with 5° step during

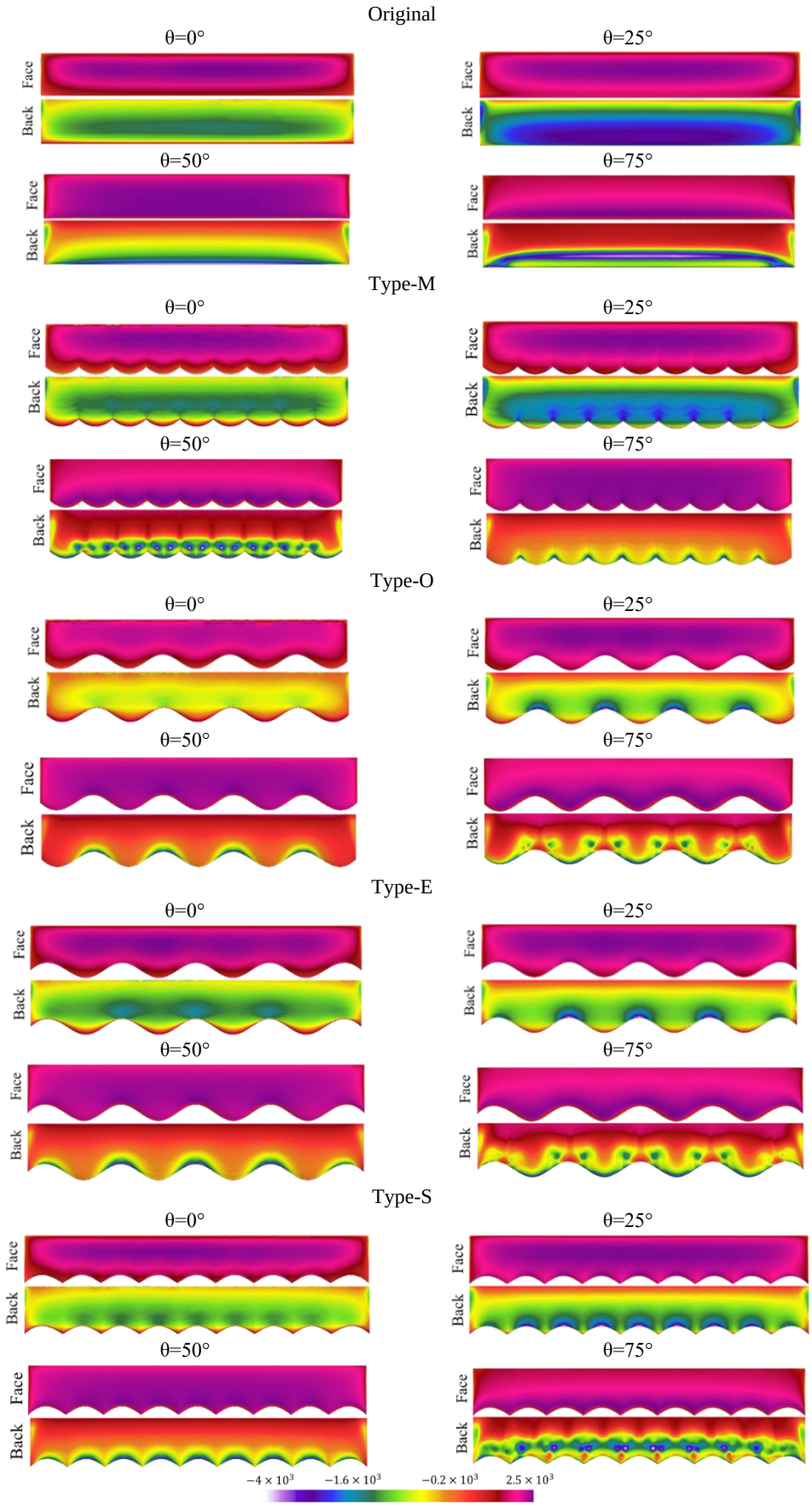

Fig. 13. Contour of pressure for all five types of oscillating hydrofoil at the various motion angles.

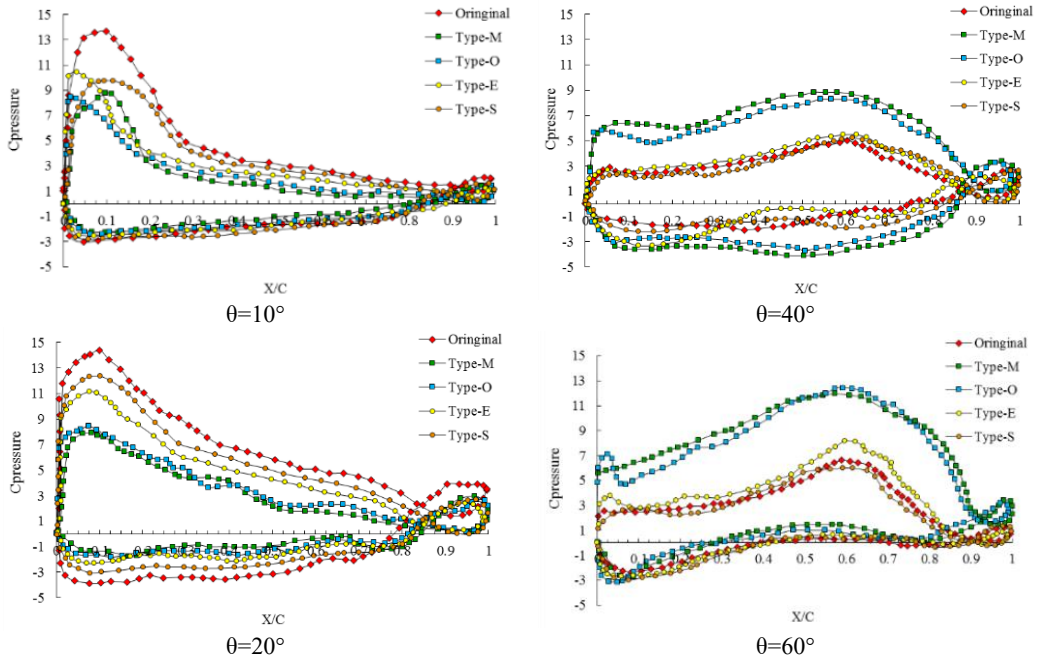

Fig. 14. Comparison of C_{press} over the midsection of all five hydrofoils under different θ, (f^*=0.12).

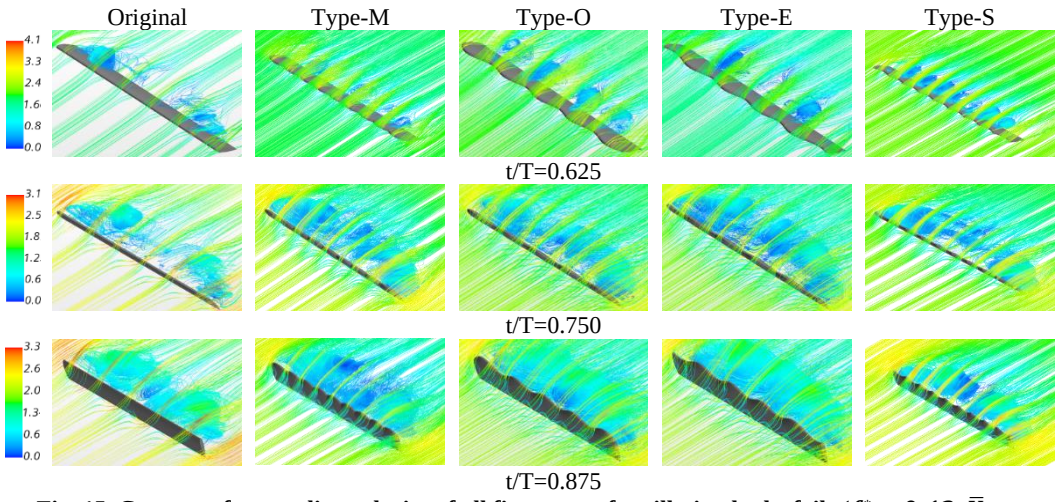

Fig. 15. Contour of streamline velocity of all five types of oscillating hydrofoils ($f^* = 0.12$, $\bar{U}_\infty = 2$ m/s).

one cycle of motion is shown in Fig. 16. It can be noted from the contours, at the AoA=35° the intensity of velocity is more than other modes. The vortex of hydrofoils at the AoA =10° and 15° is created near to hydrofoils, while at the AoA=30° and 35° is occurred far from hydrofoils at the downstream. As observed in this figure, the maximum of the vortex core appears earlier in the downstream flow when the hydrofoil has changed the angle of motion. As the pitching angle decreases the vortex is growing and the hydrodynamic performance decrease.

4.6. Vorticity contour

The important hypothesis was that the streamwise vortices induced by the wavy leading-edge enhanced the momentum exchange of the boundary layer. The flow control mode was depicted using the vortices mechanism, which is the most frequently accepted hypothesis. The trailing edge vortex (TEV) sheds from the upper surface of the hydrofoils as the hydrofoils travel upward just passing through the equilibrium position, e.g., = 10°, as displayed in Fig. 17. To better understanding of the physical phenomenon the effect of variations in leading-edge, the vorticity shape at six AoA consist of 10°, 15°, 20°, 25°, 30°, and 35° have been evaluated. The leading-edge vortex has moved to the trailing edge of the original concept but is still attached to the hydrofoil, although it has split from the changed hydrofoils, suggesting different positioning of vortex shedding with different leading-edges. The vortex behavior of the all-protuberance shapes generates counter-rotating vortices. These vortices develop in

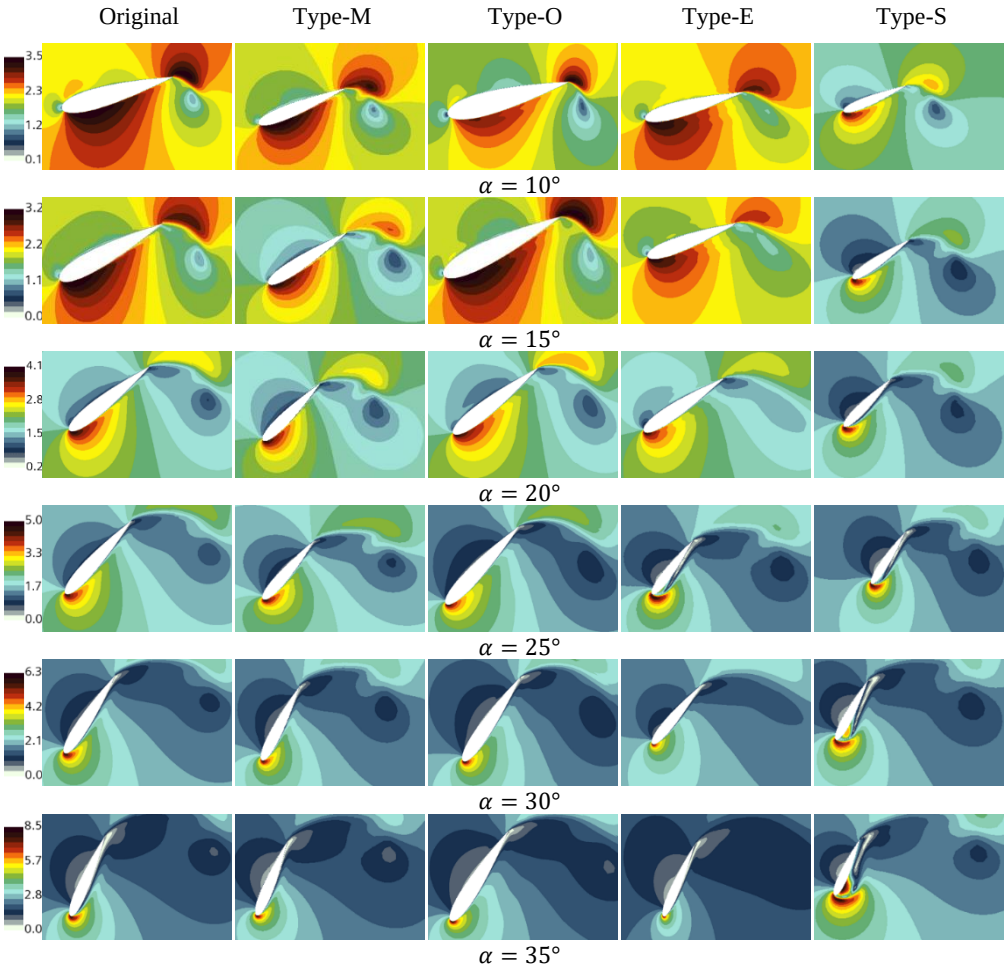

Fig. 16. Velocity contour over all five hydrofoils under different AoA (f^*=0.12).

size with a decreased intensity in the streamwise direction, similar to the behavior of vortices formed by vortex generators. Vortex strength and impacted region of Type-M are the lowest in M-Type and remarkable in other types of protuberances.

4.7. Power Extraction Efficiency

Figure 18 and Table 3 show the power extraction efficiency of hydrofoils at the reduced frequencies range of 0.08-0.16 and the inflow velocity of 2 m/s. In this study, a power extraction efficiency of 40.1% has been estimated for original case under the condition of $\bar{U}_\infty = 2$ m/s and f^*=0.12. However, for hydrofoils of Type-M, Type-O, Type-E and Type-S at the same condition the power extraction efficiency has been achieved to 46.28%, 45.01%, 43.95% and 39.26%, respectively. According to the results, the hydrofoil of Type-M has the best performance than others. In addition, numerical result shows that the efficiency of Type-O is 7-12 percent more than original hydrofoil and the efficiency of Type-E is 1-7 percent more than original hydrofoil. But, the hydrofoil of Type-S has worse performance because its efficiency during the reduced frequency of 0.09-0.15 is less than the original hydrofoil. Also, it can be seen the maximum power extraction efficiency is obtained at the reduced frequency of 0.12 for all type of hydrofoils. It can be noted from Fig. 18, the changes in the leading-edge area may improve the power extraction efficiency of hydrofoils in oscillating motion at all reduced frequency.

Table 3 Comparison of power extraction efficiency η(%) between all five types of hydrofoils, ($\bar{U}_\infty = 2\ m/s$)

f^*	0.08	0.09	0.10	0.11	0.12	0.13	0.14	0.15	0.16
Original	30.46	32.73	34.98	36.61	40.10	39.24	37.82	36.78	33.05
Type-M	33.06	36.24	38.71	43.21	46.28	44.92	43.97	40.79	36.86
Type-O	32.57	35.23	37.74	42.33	45.01	43.51	42.64	39.23	36.14
Type-E	31.98	33.17	36.05	40.19	43.95	42.73	41.37	38.68	35.10
Type-S	31.14	31.80	34.33	36.23	39.26	38.50	37.01	36.06	33.68

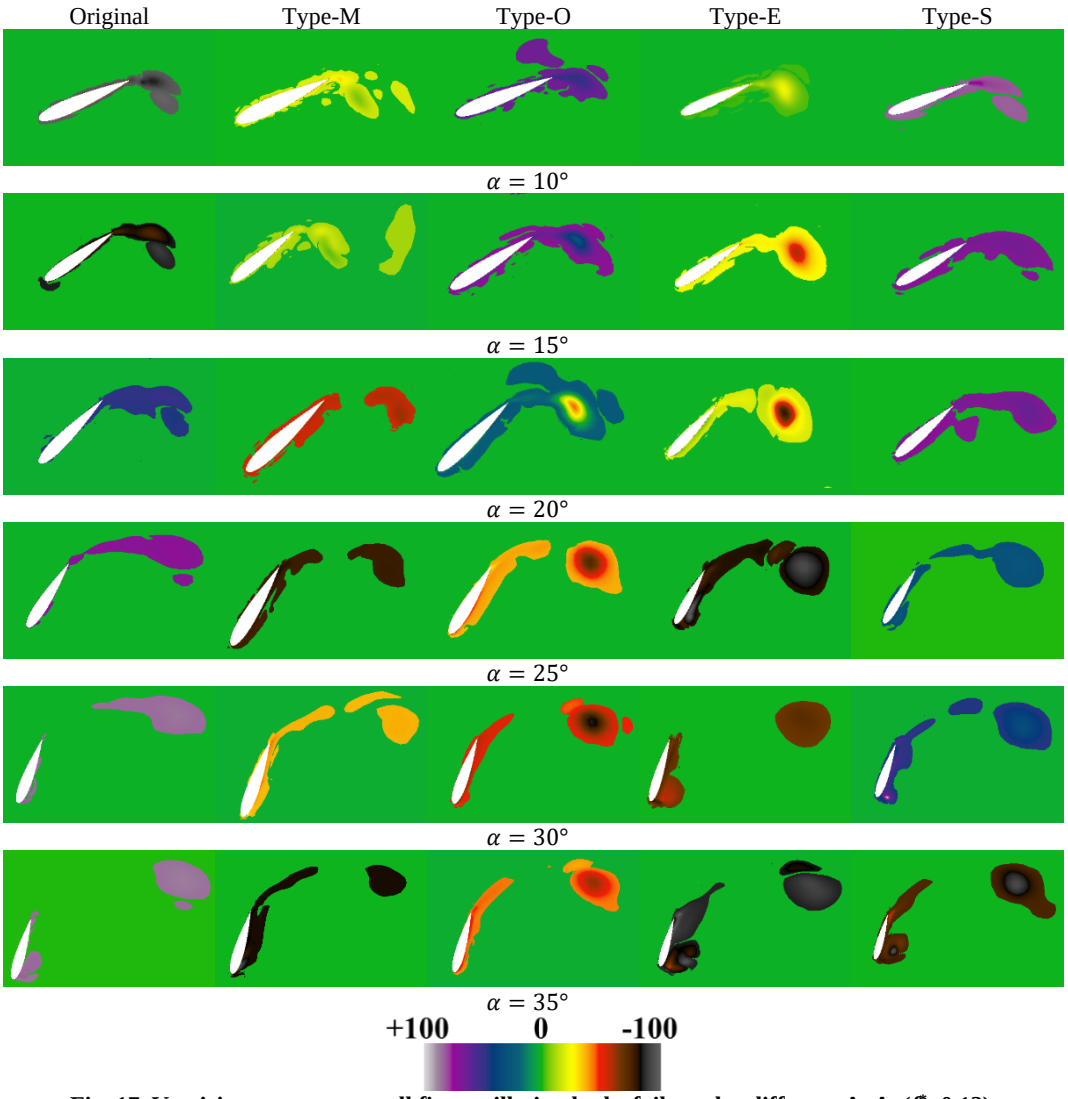

Fig. 17. Vorticity contour over all five oscillating hydrofoils under different AoA, (f^*=0.12).

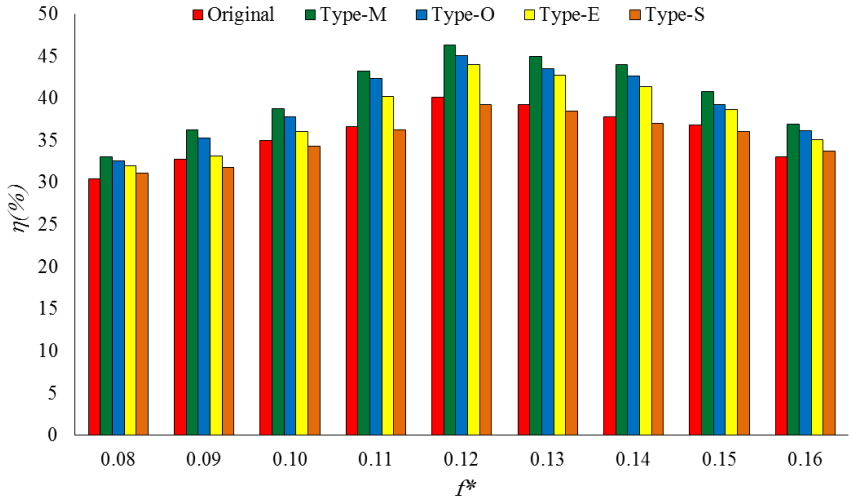

Fig. 18. Power extraction efficiency of all five types of hydrofoils against reduced frequency (flow velocity=2 m/s).

5. CONCLUSION

In this article, the hydrodynamic performance and energy extraction efficiency for five types of couples of oscillating motions (heave and pitch) hydrofoilshave been investigated. The original hydrofoil has a straight leading-edge (original) and four others have leading-edge protuberance with 9 crests (Type-M), 5 crests (Type-O), 4 crests (Type-E) and without crests (Type-S) that leading-edge forming of these hydrofoils is based on sinusoidal formulation. The numerical simulations were conducted at different reduced frequencies from 0.08 to 0.16 with an increment of 0.01 and flow velocity of 2 m/s. based on the numerical results, the following conclusion can be drawn:

- The present results of the horizontal, vertical force and power coefficients are found in good agreement with experimental data at $f^* = 0.14$, $\overline{U}_\infty = 2\ \mathrm{m/s}$.
- Among all five types, the M-type was found more efficient and had more extraction power at all reduced frequencies.
- Maximum efficiency for all types of oscillating hydrofoils is given at the reduced frequency of 0.12.
- Hydrofoil with more crest in the same span length, has better performance for all reduced frequencies during one cycle of coupled heave and pitch motions.
- Vortex strength and impacted region are the lowest in M-Type and remarkable in other types of protuberances.

REFERENCES

Abbasi, A., H. Ghassemi and D. Molyneux (2018). Numerical analysis of the hydrodynamic performance of HATST with different blade geometries. *American Journal of Civil Engineering and Architecture* 6(6), 236-241.

Abbasi, A., H. Ghassemi and D. Molyneux (2019). Power and thrust coefficients of the horizontal axis tidal stream turbine with different twist angles, blade numbers, and section profiles. *Scientific Journals of the Maritime University of Szczecin* 57 (129), 11-20.

Abbasi, A., H. Ghassemi and G. He (2021). Hydrodynamic performance of the 3D hydrofoil at the coupled oscillating heave and pitch motions. *Strojnícky Časopis - Journal of Mechanical Engineering* 71(2), 1-18.

Ashraf, M. A., J. Young, J. C. S. Lai and M. F. Platzer (2011). Numerical analysis of an oscillating-wing wind and hydropower generator. *AIAA Journal* 49(7), 1374-1386.

Boudis, A., H. Oualli, A. Benzaoui, O. Guerri, A. C. Bayeul-Laineé and O. Coutier-Delgosha (2021). Effects of non-sinusoidal motion and effective angle of attack on energy extraction performance of a fully-activated flapping foil. *Journal of Applied Fluid Mechanics* 14(2), 485-498.

Dahmani, F. and C. H. Sohn (2020). Effects of the downstream spatial configuration on the energy extraction performance of tandem/parallel combined oscillating hydrofoils. *Journal of Mechanical Science and Technology* 34(5), 2035-2046.

Derazgisoo, S. M., P. Akbarzadeh and A. Askari Lehdarboni (2019). Numerical simulation of unsteady flows with forced periodical oscillation around hydrofoils using locally power-law preconditioning method. *European Journal of Mechanics-B/Fluids* 75, 153-164.

Dropkin, A., Custodio D., Henoch C. W., and Johari H., (2012). Computation of Flowfield Around an Airfoil with Leading-Edge Protuberances. *Journal of Aircraft* 49(5), 1345-1355.

Erfort, G., T. W. Von Backström and G. Venter (2019). Numerically determined empirical relationships for a transitional turbulence model. *Journal of Applied Fluid Mechanics* 12(6), 2031-2038.

Fish, F. E. and J. M. Battle (1995). Hydrodynamic design of the humpback whale flipper. *Journal of Morphology* 225(1), 51-60.

Ganesh, N., S. Arunvinthan. S. P. Nadaraja (2019). Effect of surface blowing on aerodynamic characteristics of tubercled straight wing. *Chinese Journal of Aeronautics* 32, 1111-1120.

Gunnarson, P., Q. Zhong and D. B. Quinn (2019). Comparing models of lateral station-keeping for pitching hydrofoils. *Biomimetics* 4(3), 51.

He, G., W. Mo, Y. Gao, Z. Zhang, J. Wang, W. Wang, P. Liu and H. Ghassemi (2021). Modification of effective angle of attack on hydrofoil power extraction. *Ocean Engineering* 240, 109919.

Jamil, M., A. Javed, S. I. A. Shah, A. Hameed and K. Djidjeli (2020). Performance analysis of flapping foil flow energy harvester mounted on piezoelectric transducer using meshfree particle method. *Journal of Applied Fluid Mechanics* 13(6), 1859-72.

Javed, A., K. Djidjeli, A. Naveed and J. T. Xing (2018). Low Reynolds number effect on energy extraction performance of semi-passive flapping foil. *Journal of Applied Fluid Mechanics* 11(6), 1613–27.

Johari, H., C. Henoch, D. Custodio and A. Levshin (2007). Effects of leading-edge protuberances on airfoil performance. *AIAA Journal* 45(11), 2634-2642.

Joseph, J., S. Sridhar and S Alangar (2019). A comparison on the effect of leading edge tubercle on straight and swept wing at low reynolds number. In *46th National Conference*

on Fluid Mechanics and Fluid Power (FMFP2019), Coimbatore, India.

Kanfoudi, H., G. Bellakhall, M. Ennouri, A. Bel Hadj Taher and R. Zgolli (2017). Numerical analysis of the turbulent flow structure induced by the cavitation shedding using LES. *Journal of Applied Fluid Mechanics* 10(3), 933-46.

Karakas, F. and I. Fenercioglu (2016). Effect of side-walls on flapping-wing power- generation: An experimental study. *Journal of Applied Fluid Mechanics* 9(6), 2769–79.

Kinsey, T. and G. Dumas (2008). Parametric study of an oscillating airfoil in a power-extraction regime. *AIAA Journal* 46(6), 1318-30.

Kinsey, T. and G. Dumas (2012). Computational fluid dynamics analysis of a hydrokinetic turbine based on oscillating hydrofoils. *Journal of Fluids Engineering* 134(2).

Kinsey, T. and G. Dumas (2014). Optimal operating parameters for an oscillating foil turbine at Reynolds number 500,000. *AIAA Journal* 52(9),1885-95.

Kinsey, T., G. Dumas, G. Lalande, J. Ruel, A. Mehut, P. Viarouge, J. Lemay and Y. Jean (2011). Prototype testing of a hydrokinetic turbine based on oscillating hydrofoils. *Renewable Energy* 36(6), 1710-18.

Li, F., P. Yu, N. Deng, G. Li and X. Wu (2022). Numerical analysis of the effect of the non-sinusoidal trajectories on the propulsive performance of a bionic hydrofoil. *Journal of Applied Fluid Mechanics* 15(3), 917-25.

Li, J., C. Liu and X. Li (2021). Effects of wavy leading-edge protuberance on hydrofoil performance and its flow mechanism. *Journal of Marine Science and Engineering* 9(10).

Liu, Z., H. Qu and G. Zhang (2020). Experimental and numerical investigations of a coupled-pitching hydrofoil under the fully-activated mode. *Renewable Energy* 155,432-46.

Liu, Z., H. Qu and H. Shi (2019). Numerical study on hydrodynamic performance of a fully passive flow-driven pitching hydrofoil. *Ocean Engineering* 177, 70-84.

Mueller, M. A. and A. R. Wallace (2006). A road map for marine renewable energy research in the UK. *Journal of Marine Engineering & Technology* 5(1), 35-40.

Mumtaz Qadri M. N., A. Shahzad, F. Zhao and H. Tang (2019). An experimental investigation of a passively flapping foil in energy harvesting mode. *Journal of Applied Fluid Mechanics* 12(5), 1547-61.

Pourmahdavi, M., M. N. Safari and S. Derakhshan (2019). Numerical investigation of the power extraction mechanism of flapping foil tidal energy harvesting devices. *Energy & Environment* 30(2), 193-211.

Qi, Z., J. Zhai, G. Li and J. Peng (2019). Effects of non-sinusoidal pitching motion on the propulsion performance of an oscillating foil. *PloS One* 14(7), e0218832.

Reddy, C. J. and A. Sathyabhama (2023). Comparative study on the effect of leading edge protuberance of different shapes on the aerodynamic performance of two distinct airfoils. *Journal of Marine Science and Engineering* 16(1), 157-177.

Ribeiro, B. L. R., S. L. Frank and J. A. Franck (2020). Vortex dynamics and Reynolds number effects of an oscillating hydrofoil in energy harvesting mode. *Journal of Fluids and Structures* 94, 102888.

Rostami, A. B. and M. Armandei (2017). Renewable energy harvesting by vortex-induced motions: Review and benchmarking of technologies. *Renewable and Sustainable Energy Reviews* 70, 193-214.

Segura, E., R. Morales and J. A. Somolinos (2018). A strategic analysis of tidal current energy conversion systems in the European Union. *Applied Energy* 212, 527-51.

Srinivas, K. S., A. Datta, A. Bhattacharyya and S. Kumar (2018). Free-stream characteristics of bio-inspired marine rudders with different leading-edge configurations. *Ocean Eng.* 170, 148-159.

Utama, I., D. Satrio, M. Mukhtasor, W. Atlar, R. H. Shi and G. Thomas (2020). Numerical simulation of foil with leading-edge tubercle for vertical-axis tidal-current turbine. *Journal of Mechanical Engineering and Sciences* 14(3), 6982-6992.

Wei, Z., T. H. New and Y. D. Cui (2015). An experimental study on flow separation control of hydrofoils with leading-edge tubercles at low Reynolds number. *Ocean Engineering* 108, 336-349.

Wu, X., X. Zhang, X. Tian, X. Li and W. Lu (2020). A review on fluid dynamics of flapping foils. *Ocean Engineering* 195, 106712.

Xiao, Q. and Q. Zhu (2014). A review on flow energy harvesters based on flapping foils. *Journal of Fluids and Structures* 46, 174-91.

Xu, J., H. Zhu, D. Guan and Y. Zhan (2019). Numerical analysis of leading-edge vortex effect on tidal current energy extraction performance for chord-wise deformable oscillating hydrofoil. *Journal of Marine Science and Engineering* 7(11).